8th ANKARA INTERNATIONAL AEROSPACE CONFERENCE
10-12 September 2015 - METU, Ankara TURKEY

AIAC-2015-117

FORCE MEASUREMENTS AND ESTIMATION BASED ON DPIV DATA FOR A PLUNGING FLAT PLATE

Emre TURAM[1], Onur PAÇA[2], Idil FENERCIOGLU[3] and Okşan ÇETİNER[4]
Istanbul Technical University
Istanbul, Turkey

ABSTRACT

Simultaneous Force/Torque and quantitative velocity measurements are performed in a water channel for a sinusoidally plunging flat plate model. The flow structures in the near wake of the plunging flat plate are first addressed qualitatively using DPIV results and then direct force measurement results are taken into consideration for drag/thrust production. Forces acting on the plunging flat plate are also estimated using DPIV data. The added-mass force acting on the plunging flat plate is analytically calculated and considered for the efficiency of the flapping.

INTRODUCTION

Low Reynolds number flows are receiving considerable attention due to the possible application areas related to micro-air-vehicles (MAV). Biological inspiration is a recent interest to enhance the performance of the next generation of small-scale air vehicles over existing fixed and rotary wing systems. Researchers aim to employ the unsteady mechanisms of flapping wings to overcome the unfavorable aerodynamic conditions and the unsteady flows in low Reynolds number regimes gain increasing attention in recent years.

Due to the simplicity of the motion, the earliest theories concerning flapping wing flight are related to purely heaving airfoils. The theory of thrust generation using flapping foils was first proposed by Knoller [1909] and Betz [1912] and then experimentally confirmed by Katzmayer [1922]. The Knoller-Betz theory states that a harmonically plunging wing in a freestream flow results in generation of an effective angle of attack and when the airfoil is oscillated at sufficiently high amplitude and frequency, the downstream velocity distribution becomes jet-like and thus is indicative of a net thrust on the airfoil.

Jones et al. [1998] demonstrated the Knoller-Betz effect by performing flow visualization experiments in the wake of a purely plunging airfoil model and according to positions of shed vortices, they classified their results as drag producing, neutral, thrust producing and dual-mode thrust producing categories. They defined the non-dimensional plunge velocity by the multiplication of the reduced frequency (k) and the non-dimensional plunging amplitude (h) which essentially has the same meaning as Strouhal number in characterizing the type of vortex shedding in the wake of a flapping airfoil. As given in Figure 1, plunge amplitude times reduced frequency value is plotted as a constant dividing line between the drag producing and thrust producing parameters for a single plunging airfoil.

[1] Undergraduate student in Aeronautical Engineering Department, Email: turam@ itu.edu.tr
[2] Graduate student in Aeronautical and Astronautical Engineering Department, Email: paca@itu.edu.tr
[3] Post Doc Researcher/Lecturer in Astronautical Engineering Department, Email: fenercio@itu.edu.tr
[4] Professor in Astronautical Engineering Department, Email: cetiner@itu.edu.tr

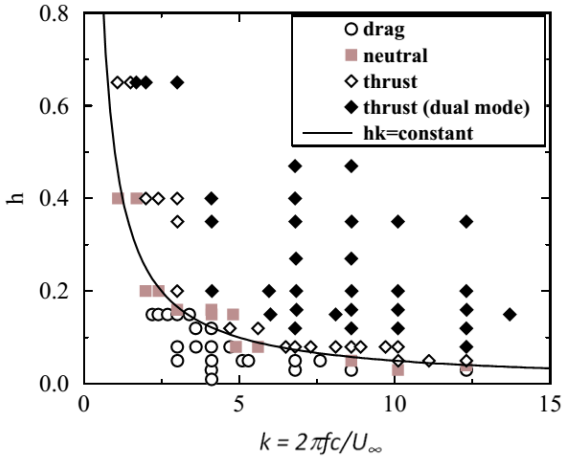

Figure 1. *Drag/Thrust as a function of h and k [Jones et al. 1996]*

Similar occurrence for the threshold of thrust producing wake was also observed in a previous study by Fenercioglu and Cetiner [2012], where they categorized the flow structures around and in the near wake of the airfoil based on different independent parameters, obtained from quantitative flow field measurements using DPIV (Digital Particle Image Velocimetry) method in a water channel for a pitching and plunging airfoil in a range applicable to Micro Air Vehicles (MAVs). In the preceding study, average thrust force and efficiency are estimated from the DPIV velocity data by simply using the wake excess velocity and the momentum theorem, using the steps provided by Anderson et al. [1998] ([Fenercioglu, 2010]). The same water channel facility and the same airfoil kinematics were used in recent studies by Karakas et al. [2014] and Caylan et al. [2014] where simultaneous direct force acquisitions were performed in addition to DPIV measurements. One of the major problems encountered in direct force acquisition in water channels is the added mass effect, the ratio of this added mass force to the total measured force needs to be revealed in order to comment on the net force acting on a flapping airfoil, therefore the efficiency of flapping. In the aforementioned previous studies, the added mass effect was prevailing particularly for the cases with higher thrust production and lessens for the cases with lower thrust and higher efficiency values. In those studies the airfoil's combined flapping motion was dominated by the plunging component, as also given in Fenercioglu and Cetiner [2014], thus the focus of the current investigation is on simple plunging motion to take into account the contribution of the added mass in the direct force measurements.

The potential of using the velocity vector field obtained by DPIV method to calculate the time dependent forces acting on a plunging airfoil was demonstrated by Violato et al. [2011] and van Oudheusden [2013]. Obtaining force values from flow field data also draws considerable global attention; a current European Union FP7 project NIOPLEX (Non-intrusive Optical Pressure and Loads Extraction for Aerodynamic Analysis) is interested in estimating forces based on DPIV data for oscillating airfoils. A preliminary study by Turam et al. [2014] was conducted in a water channel to determine the temporal and spatial resolution required for pressure and force estimations from DPIV data.

The aim of this study is to determine the value of the added mass contribution in the total force measurements to reveal the net force acting on a flapping foil. For the analytical calculation of the added mass, the flapping motion of the test model is considered as pure plunging motion and the formulation given by Naudascher and Rockwell [2005] is used. This experimental study comprises simultaneous direct force measurements along with DPIV data acquisition for the validation purposes of the estimated force values at low Reynolds number range applicable to Micro Air Vehicle operations.

EXPERIMENTAL SETUP

The experiments are conducted in the large scale, free surface water channel located in the Trisonic Laboratory of Istanbul Technical University Aeronautical and Astronautical Engineering Department. A flat plate is mounted in a cantilevered arrangement from its mid-chord position inside the water channel between two end plates to reduce the free surface and end effects. The mounting beam is connected to a linear table which allows the plunging motion. The Plexiglas flat plate has a chord (c) of

10cm and span (*s*) of 30cm. The experimental arrangement can be seen in Figure 2. DPIV (Digital Particle Image Velocimetry) technique is used to record flow fields around the cylinder and therefore to analyze the vortical structures and the velocity field. The flow is illuminated by a dual cavity Nd:Yag laser (max. 120mJ/pulse) and the water is seeded with silver coated hollow glass spheres with a mean diameter of 10 μm. The velocity fields around and in the near wake of the plunging flat plate are obtained using two 10-bit cameras with 1600 × 1200 pixels resolution, positioned underneath the water channel. Recorded images are stitched using an in-house code and then interrogated using a double frame, cross-correlation technique with a window size of 64 × 64 pixels and 50% overlapping in each direction. For each case, 1200 vector fields are recorded during 30 cycles of plunge motion. Therefore, for each cycle of motion, 40 vector fields are used to estimate the loads.

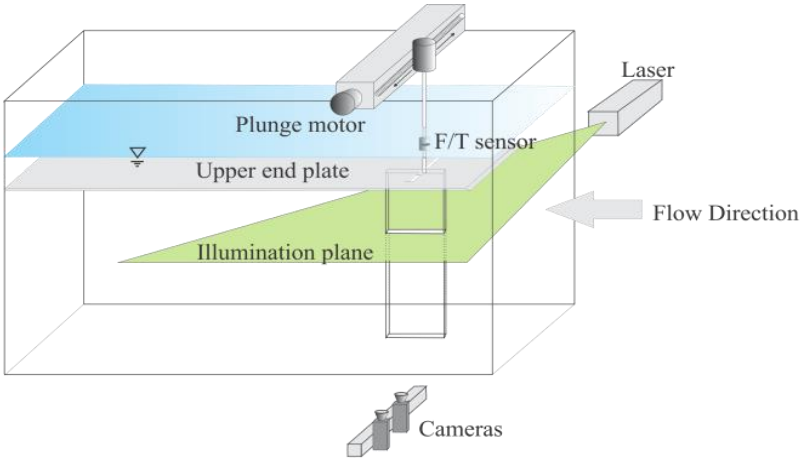

Figure 2. *Experimental setup*

Force and moments acting on the plunging flat plate are measured using a six-component ATI NANO-17 IP68 Force/Torque (F/T) sensor. The sensor is attached to the vertical cantilevered mounting beam of the test model, oriented with its cylindrical z-axis normal to the pitch-plunge plane. The plunge motion of the model is accomplished with Kollmorgen/Danaher Motion AKM54K servo motor which was connected to a computer via ServoSTAR S700 digital servo amplifier. Motor motion profiles are generated by a signal generator Labview VI (Virtual Instrument) for the given amplitude and frequency. The same VI triggered the PIV system at the beginning of the third motion cycle of the airfoil and synchronization is achieved using a National Instruments PCI-6601 timer device. The sinusoidal plunging motion of the airfoil is given as;

$$h(t) = h_{\text{amp}} \sin(2\pi f t)$$

where $h(t)$ is the linear plunge motion, transverse to the freestream velocity, h_{amp} is the plunge amplitude and f is the plunging frequency.

The reduced frequency (k) is defined as:

$$k = \frac{2\pi f c}{U_\infty}$$

where U_∞ is the freestream velocity.

The occurrence of Drag and Thrust producing wake for a plunging airfoil as a function of the plunging amplitude and the reduced frequency is re-illustrated in Figure 3 based on the data by Jones et al. [1996]. The test case points for the present study are also marked with triangular symbols on the same plot.

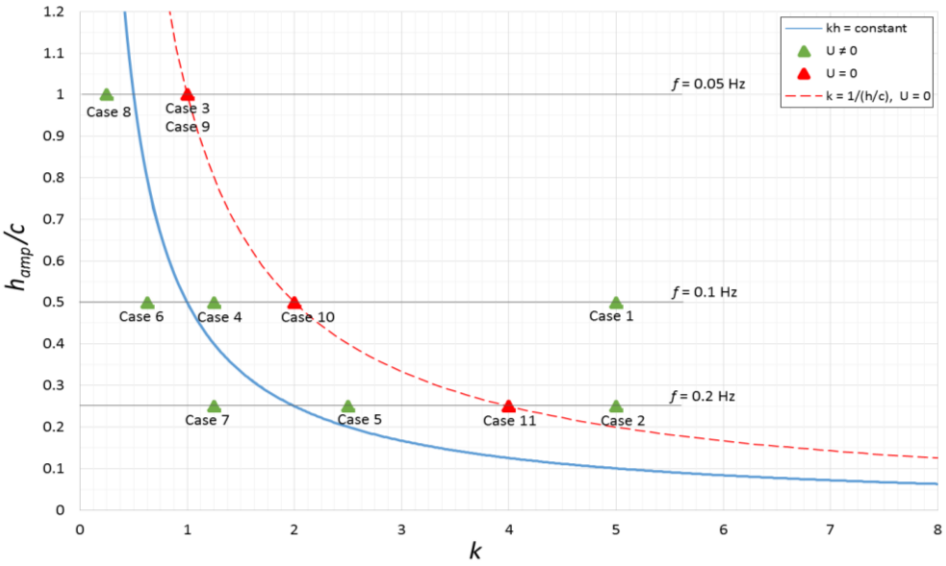

Figure 3. *Investigated test cases*

The investigated points as given in the plot include both drag cases and thrust cases placed on both sides of the dividing *hk* constant line as well as cases of interest to the EU-FP7 project NIOPLEX. The plunge-only equivalent cases of the initially pitching and plunging airfoil as tested in Fenercioglu and Cetiner [2012] were also included. The tests were also repeated without the free-stream velocity, those special cases lie on the $k = 1/(h/c)$ constant line. For all cases, DPIV and force/moment data are acquired simultaneously. The tare measurements were also obtained in air with the same motion kinematics of each case. The test case parameters are given in Table 1. The Reynolds number for cases where the flat plate plunges in quiescent fluid is expressed based on the maximum plunging velocity.

Table 1. *Investigated test case parameters*

Exp. No.	Category	Re	*U* [m/s]	*f* [Hz]	$k=2\pi fc/U$	h_{amp}/c	h_{amp}
Case 1	pseudo A1	1250	0.013	0.1	5.01	0.50	50
Case 2	pseudo B2	2500	0.025	0.2	5.01	0.25	25
Case 3	ET2	3125	0.031	0.05	1.00	1.00	100
Case 4	Nio4	5000	0.050	0.1	1.25	0.50	50
Case 5	Nio1- pseudo D	5000	0.050	0.2	2.50	0.25	25
Case 6	pseudo E	10000	0.100	0.1	0.63	0.50	50
Case 7	Nio2	10000	0.100	0.2	1.25	0.25	25
Case 8	ET1	12500	0.126	0.05	0.25	1.00	100
Case 9	0 velocity water-f=0.05	3129	0.031	0.05	1.00	1.00	50
Case 10	0 velocity water-f=0.1	3129	0.031	0.1	2.00	0.50	50
Case 11	0 velocity water-f=0.2	3129	0.031	0.2	4.00	0.25	25

FORCE ESTIMATION

Forces on the plunging plate are calculated using the Reynolds Transport Theorem written for the linear momentum. The equation involves the integration of flow variables inside and around a control volume surrounding the flat plate. The lift and drag forces are expressed in the following equation given by Kurtulus et al. [2007], neglecting the viscous term as in most of the cases Re>1000 [Violato et al., 2011].

$$\begin{bmatrix} D \\ L \end{bmatrix} = -\rho \iint\limits_{V} \begin{bmatrix} \frac{\partial u}{\partial t} dxdy \\ \frac{\partial v}{\partial t} dxdy \end{bmatrix} + \rho \oiint\limits_{S} \begin{bmatrix} -u^2 dy + uvdx \\ -uvdy + v^2 dx \end{bmatrix} + \oint\limits_{S} \begin{bmatrix} -pdy \\ pdx \end{bmatrix}$$

The pressure term in the above quation is calculated by the explicit integration of planar pressure gradients obtained by the use of incompressible Navier-Stokes Equations in two-dimensional form. Eulerian and Lagrangian approaches are successively used for the computation of the material derivative in the Navier-Stokes Equations.

The temporal and spatial resolutions for force estimation are determined based on a previous preliminary study by Turam et al. [2014]. According to the sensitivity analyses performed on Case-5 (Nio1), a spatial resolution of 3% of the chord and a field of view covering all the amplitude of motion give satisfactory results with a temporal resolution expressed as 40 vector fields per cycle of motion. In terms of DPIV post-processing, average correlation is found to reduce the noise as it is expected. On the other hand, the estimated load matched better the direct measurement when it is phase averaged and filtered. It should be noted that the compared direct measurement results are also 1 Hz filtered.

RESULTS

The results will be presented in three sub-sections involving the DPIV, the direct force measurments and the force estimation results.

Digital Particle Image Velocimetry (DPIV) Results

Below, adopted from Fenercioğlu [2010], there is a template (Figure 4) for the following two figures presenting instantaneous vorticity patterns around the model. The first image is at the right hand side of the figure where the model is at its mid-plunge position. The plate first moves upward and then images 3 to 7 represent the downstroke. The ninth image on the left hand side represents the beginning of the following cycle of motion. The images are aligned on a sinusoidal curve. As the flow is from left to right in the experiments, the figure simulates the forward motion of the model from right to left. However, the amplitude and period of the curve is not scaled with the actual motion due to the limitation of the page layout. The first image on the figure is the beginning of the fourth cycle of the motion from the startup for both cases.

In Figures 5 and 6, the results of the current study are on the left hand side, while the equivalent case results of a pitching and plunging SD7003 [Fenercioglu and Cetiner, 2012] are given on the right hand side. Figure 5 represents Case-1, flow structure category of A1 as described in Fenercioglu and Cetiner, [2012]. Figure 6 represents Case-2, flow structure category of B2 as described in Fenercioglu [2010]. Although the SD7003 undergoes a combined pitch and plunge motion, the flow structure similarity for both cases are remarkable. At the given Reynolds numbers and motion parameters, the flow is highly plunge dominated and insensitive to the model profile. It should be noted that the SD7003 airfoil undergoes combined pitching and plunging oscillations with a phase difference of $\pi/2$ where pitch leads the plunge motion. The initial angle of attack of the motion is 8° and the pitching amplitude is 8.6°. This similarity between the flow structures is observed nearly for all cases, however it is lost when the freestream speed is increased and the case gets closer to the drag region, e.g. for Case-6.

The average velocity and vorticity fields for all cases are given in Figure 7. The figure reveals either drag or thrust production by means of momentum deficit or jet-like formation from the velocity field in the near-wake; the vortical structures show also Karman-like formation or a reverse Karman street. The figure also includes the corresponding freestream velocity vector for each case on top of each image. For cases ran in quiescent fluid, a reference vector corresponding to Re=10000 is presented to show the strength of the jet-like formation for comparison. Qualitatively, it possible to distinguish Case-1, Case-2, Case-3 and Case-4 as thrust producing cases although the thrust is expected to be lower based on the diminishing strength of the jet-like formation. On the other hand, Case-6, Case-7 and Case-8 are clearly on the drag side with a momentum deficit in the near-wake and clockwise vortices on the upper side of the plunge centerline. Case-10 and Case-11 are evidently among thrust producing cases when the freestream speed is zero. For Case-5 and Case-9, it is not possible to make an unbiased comment. Both cases lay on the thrust side, close to the dividing line between

thrust and drag occurrence. Case-5 shows jet-like formation at the centerline of the plunge motion, however a clockwise vortex is present on the upper side. Although Case-9 does not present a distinct jet-like formation, the clockwise vortex formation appears on the lower side of the plunge centerline, nearly at the edges of the field of view with its counterpart. Actually this is in accord with both Figure 1 and Bohl and Koochesfahani [2009] who studied the effect of velocity fluctuations in the integration of the momentum theorem for pure pitch oscillations and showed that the switch in the vortex array orientation does not coincide with the condition for crossover from drag to thrust.

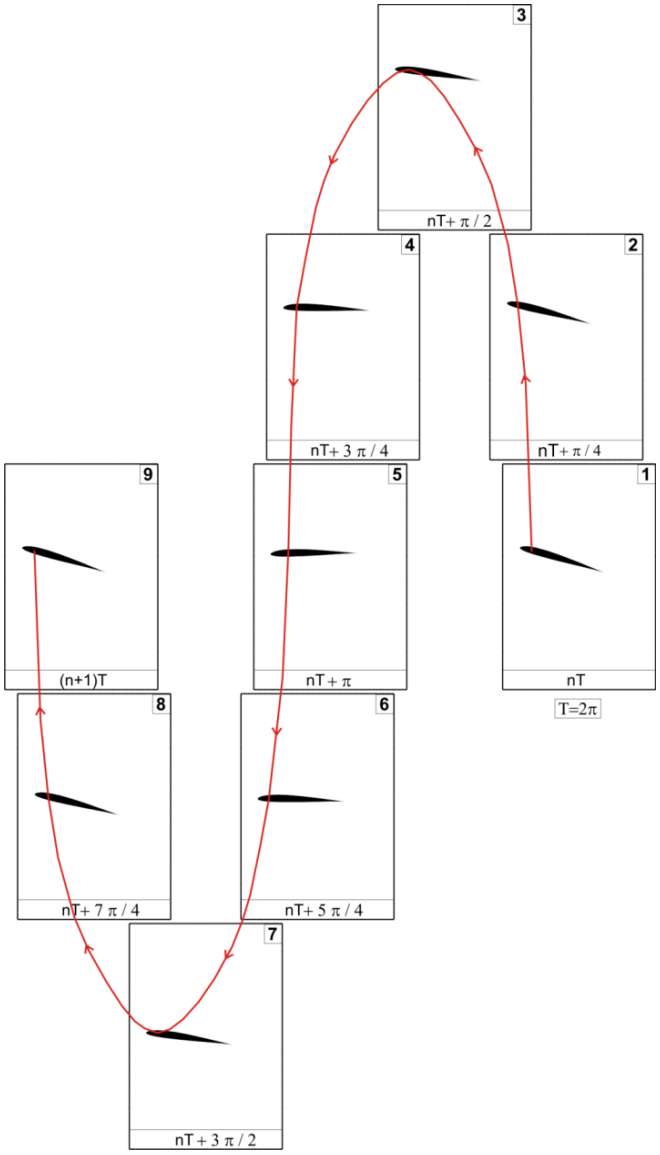

Figure 4. *Template for figures showing instantaneous vorticity patterns*

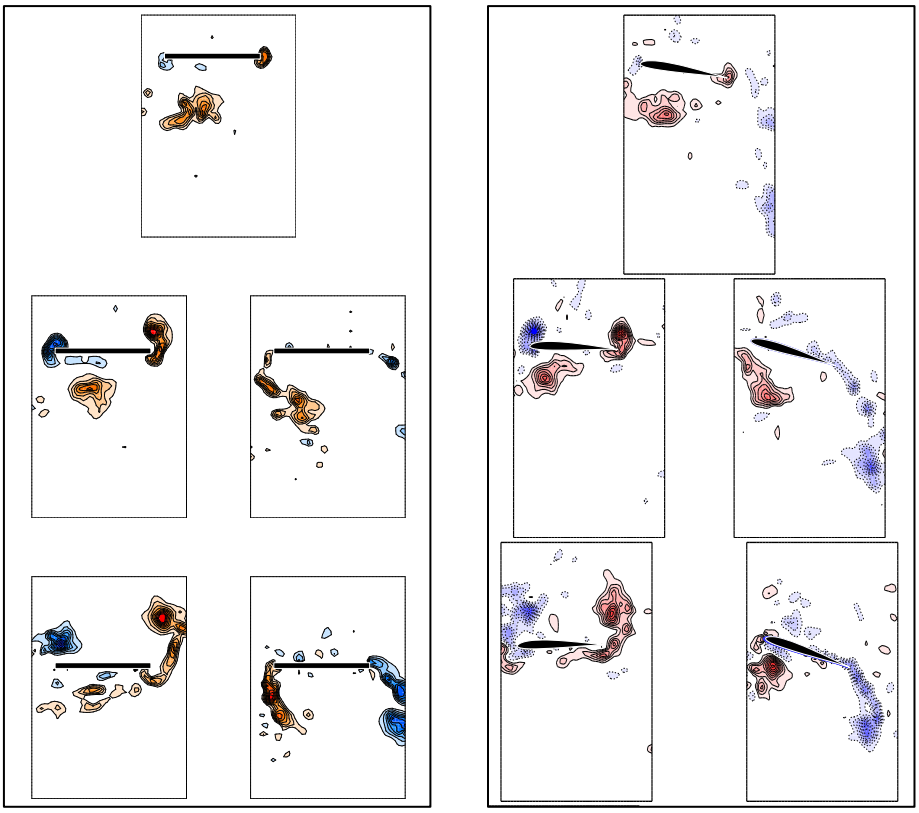

(a) **(b)**

Figure 5. *Instantaneous vorticity patterns for half period of motion during upstroke for a) plunging flat plate for Case-1, b) pitching and plunging SD7003 airfoil (Category-A1)*

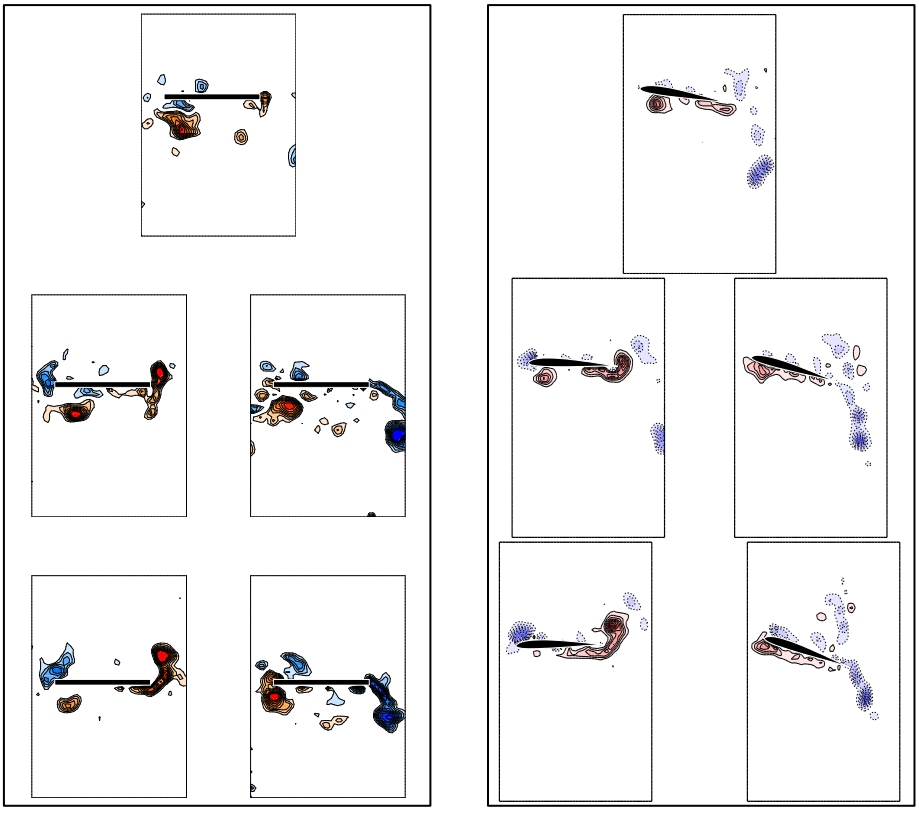

(a) **(b)**

Figure 6. *Instantaneous vorticity patterns for half period of motion during upstroke for a) plunging flat plate for Case-2, b) pitching and plunging SD7003 airfoil (Category-B2)*

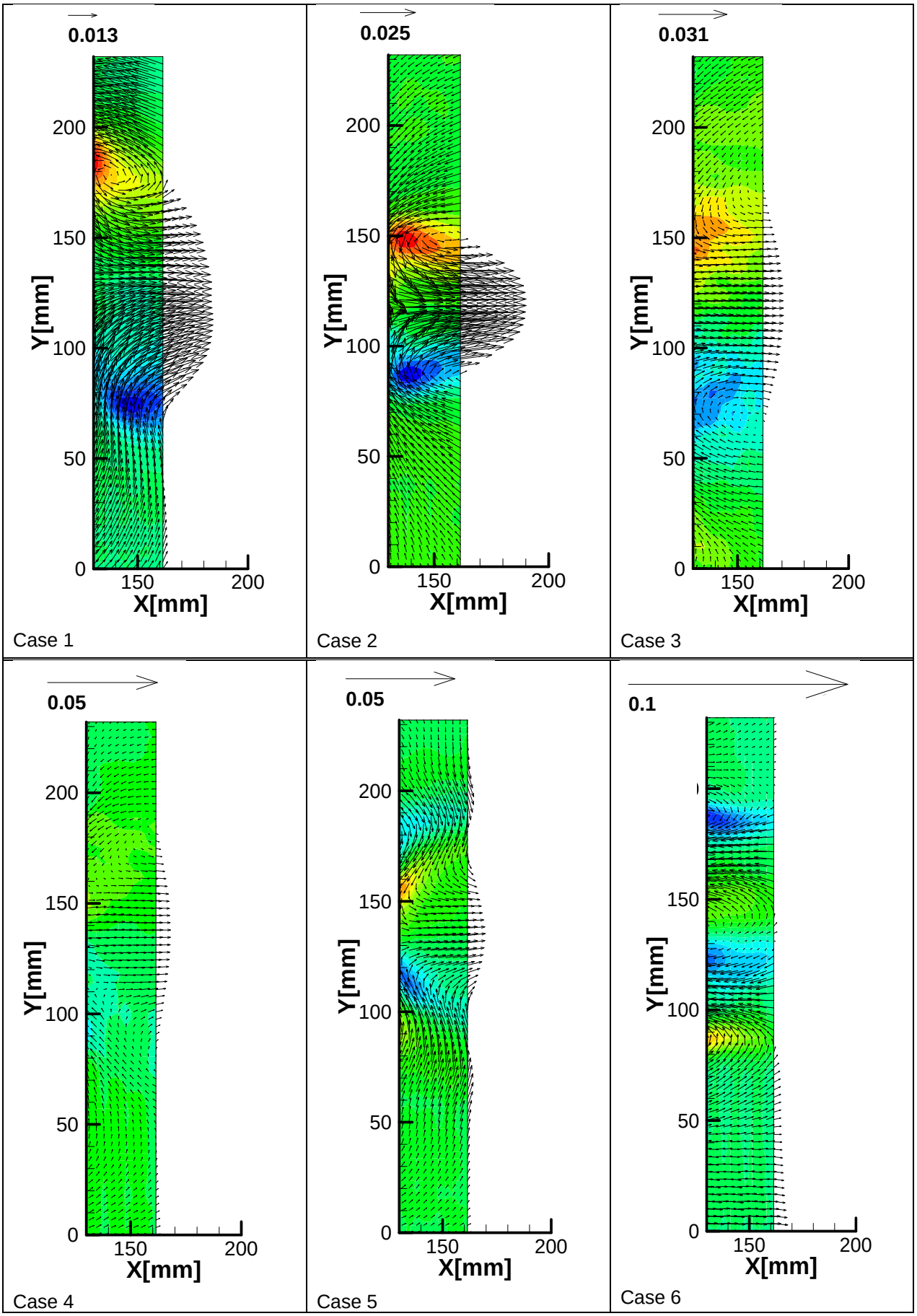
0.013
0.025
0.031
0.05
0.05
0.1
Y[mm]
X[mm]
0
50
100
150
200
Case 1
Case 2
Case 3
Case 4
Case 5
Case 6

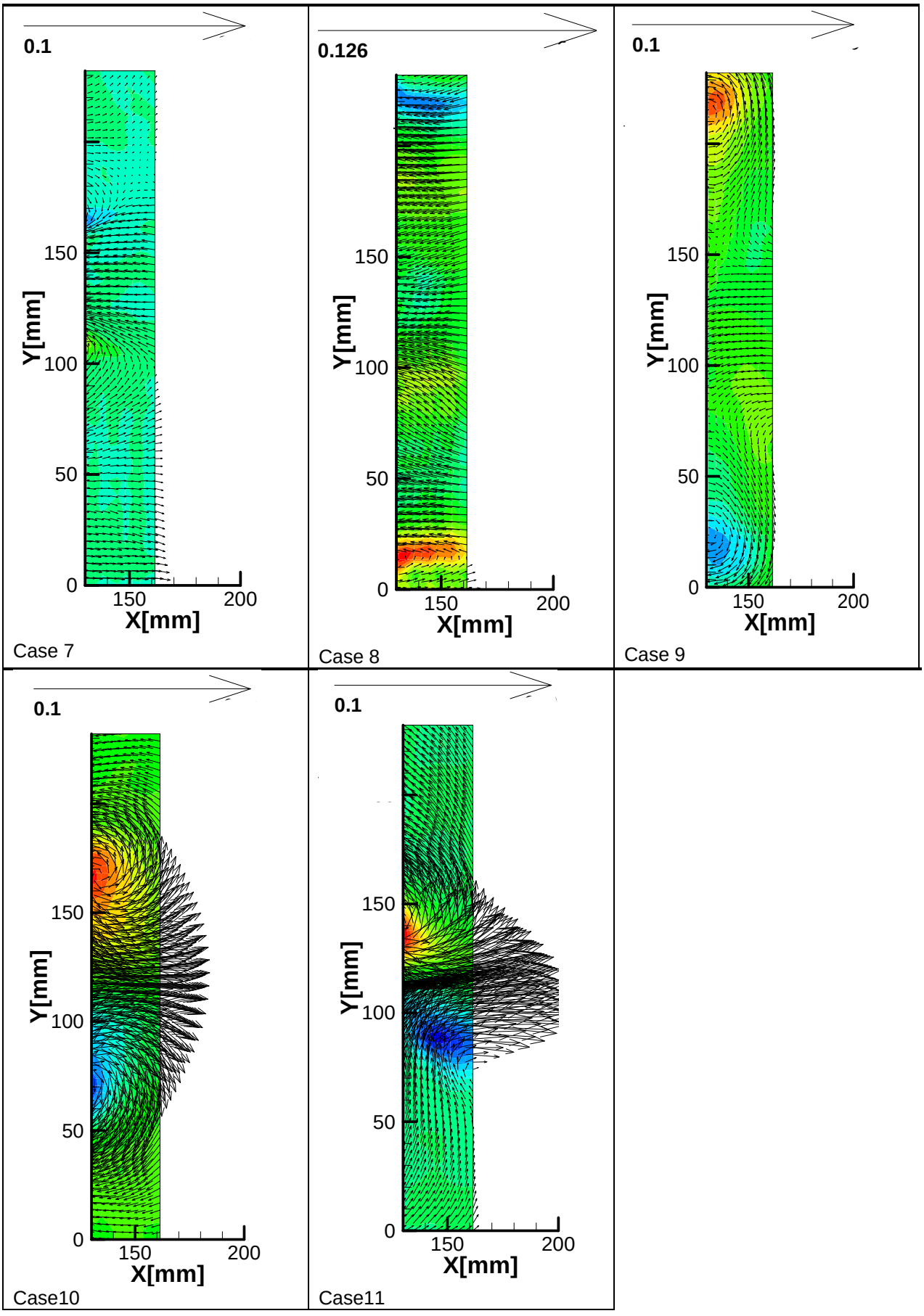

Figure 7. *Average velocity and vorticity fields for all cases*

Direct Force Measurements Results

Lift and drag force measurement results, both dimensional and non-dimensional values are given in Table 2. Drag forces are in general very low, in the order of the measurement device resolution and even below for Case 5 and Case 9. Negative values indicate thrust and those cases producing thrust are colored green while those yielding drag are colored orange. The bold font indicates the most reliable values. Although it may be questionable to be based on the drag results, interestingly the average values in order, given in Table 3, coincide with the qualitative results. For the two cases, namely Case 5 and Case 9, the drag force is nearly zero and in accordance with that, the DPIV results do not yield qualitatively any unbiased conclusion on either drag or thrust occurrence.

Table 2. *Direct force measurement results*

Exp No	Category		L (N)	D (N)	CL	CD
Case 1	pseudo A1	min	-0.1090	-0.0077	-43.0036	-3.0287
		max	0.0858	-0.0026	33.8468	-1.0396
		ave	-0.0054	-0.0053	-2.1443	-2.0970
Case 2	pseudo B2	min	-0.1317	**-0.0153**	-14.0432	-1.6283
		max	0.1334	**-0.0030**	14.2271	-0.3203
		ave	0.0025	**-0.0088**	0.2680	-0.9336
Case 3	ET2	min	-0.0463	-0.0104	-3.2134	-0.7236
		max	0.1044	-0.0030	7.2448	-0.2076
		ave	0.0294	-0.0056	2.0414	-0.3851
Case 4	Nio4	min	-0.0937	-0.0075	-2.4985	-0.1994
		max	0.1061	0.0005	2.8286	0.0146
		ave	0.0065	-0.0025	0.1743	-0.0675
Case 5	Nio1	min	-0.1178	-0.0045	-3.1421	-0.1208
		max	0.1315	0.0071	3.5072	0.1881
		ave	0.0078	0.0018	0.2093	0.0480
Case 6	pseudo E	min	-0.2214	**0.0003**	-1.4758	0.0023
		max	0.2222	**0.0157**	1.4813	0.1045
		ave	0.0014	**0.0091**	0.0095	0.0606
Case 7	Nio2	min	-0.1710	-0.0008	-1.1398	-0.0053
		max	0.1980	0.0106	1.3203	0.0708
		ave	0.0130	0.0056	0.0866	0.0372
Case 8	ET1	min	-0.3042	**0.0075**	-1.2776	0.0317
		max	0.3046	**0.0315**	1.2791	0.1323
		ave	0.0050	**0.0196**	0.0210	0.0821
Case 9	0 vel - water-f=0.05	min	-0.0945	-0.0021	-6.3891	-0.1436
		max	0.1036	0.0022	7.0070	0.1497
		ave	0.0062	0.0003	0.4165	0.0177
Case 10	0 vel - water-f=0.1	min	-0.1407	-0.0069	-9.5112	-0.4679
		max	0.1527	-0.0021	10.3249	-0.1383
		ave	0.0098	-0.0041	0.6606	-0.2741
Case 11	0 vel - water-f=0.2	min	-0.1766	-0.0082	-11.9435	-0.5569
		max	0.1905	-0.0032	12.8821	-0.2151
		ave	0.0115	-0.0052	0.7764	-0.3489

On the other hand, it is possible to comment on the lift force measurements as they are considerably large in comparison with the drag force results. In some cases, e.g. Case 1 and Case 2, the lift force coefficient is remarkably large. Half of the peak to peak values for both lift and added-mass coefficient variations are presented in Table 4, the values in the order from largest to smallest. In general, the cases with large lift coefficient experience also large added-mass forces. Considering that added-mass force is proportional to the square of the motion frequency, for a given motion amplitude, the added-mass force increases in the thrust region of h-k plot when we get far from the dividing line between thrust and drag occurrence. Since in this study, different reduced frequency values are obtained changing the freestream values for a given motion amplitude, it is possible to conclude that high thrust is produced when the added-mass force experienced by the flapping wing is large.

Table 3. *Thrust and drag occurrence order*

Exp No	CD
Case 1	-2.0970
Case 2	-0.9336
Case 3	-0.3851
Case 11	-0.3489
Case 10	-0.2741
Case 4	-0.0675
Case 9	0.0177
Case 7	0.0372
Case 5	0.0480
Case 6	0.0606
Case 8	0.0821

Table 4. *Added-mass and lift coefficients*

Exp No	CA
Case 1	18.3468
Case 2	9.9218
Case 11	6.2894
Case 10	3.1448
Case 5	2.4805
Case 3	1.6132
Case 9	1.5724
Case 4	1.2402
Case 7	0.6201
Case 6	0.3101
Case 8	0.0977

Exp No	CL
Case 1	38.4252
Case 2	14.1351
Case 11	12.4128
Case 10	9.9180
Case 9	6.6981
Case 3	5.2291
Case 5	3.3246
Case 4	2.6636
Case 6	1.4785
Case 8	1.2783
Case 7	1.2301

Force Estimation Results

As indicated by Jardin et al. [2009], on the contrary to the lift evaluation, the drag prediction by means of the momentum equation approach is subjected to specific difficulties linked to the pressure contribution evaluation. On the other hand, it is also reported in Jardin et al. [2009] that the viscous term may be neglected if the control surface is sufficiently far away from the body in motion. Although the viscous term is neglected in this study based on the Reynolds numbers investigated, the control surface is not always sufficiently far away from the plunging flat plate. As the force estimation results for drag are not considered successful and the direct force measurement results to be compared with for the drag variation are not reliable, only estimation of lift force variations will be presented herein.

Although 30 cycles of motion are recorded for each case, the force estimation code is ran, for the time being, for 3 cycles of motion and the results are evaluated based on instantaneous estimations despite the fact that phase averaging and filtering or average correlation are found to decrease the fluctuations in the results and give a better estimate. Figure 8 shows selected four cases where best performance of the estimation code is obtained under aforementioned conditions. Interestingly, three cases out of four constitutes all the plunge cases performed at the lowest plunge frequency and for largest plunge amplitude. Although, the estimation code is still under development and requires improvement, these preliminary results can be considered successful taking account that even a mature code ran using a 3D velocity data may deviate considerably for some parts of the motion cycle as in the study of Tronchin et al. [2015].

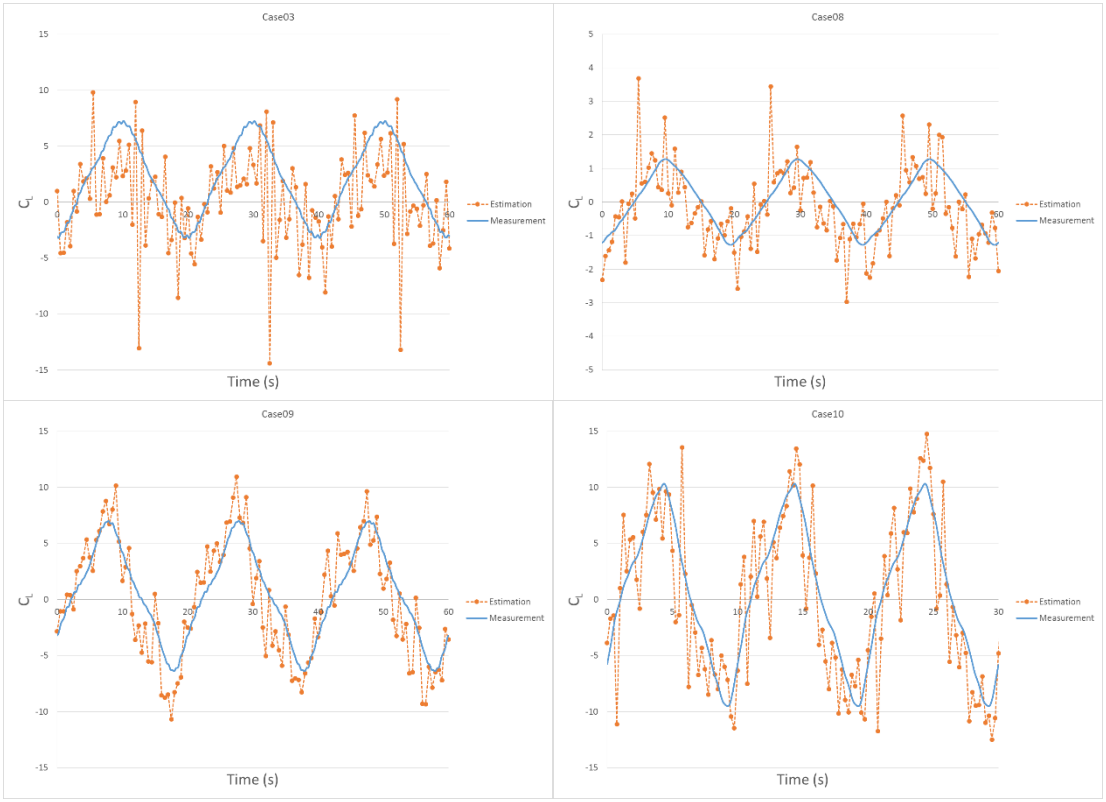

Figure 8. *Force estimation results for selected four cases*

CONCLUSIONS

A comprehensive study for the measurement and/or the estimation of forces in flapping wing aerodynamics is underway to provide further insight into the flow physics and the efficiency in flapping motion. Simultaneous Force/Torque and quantitative velocity measurements are performed in a water channel for a sinusoidally plunging flat plate model. The flow structures in the near wake of the plunging flat plate are first addressed qualitatively using DPIV results and then direct force measurement results are taken into consideration for drag/thrust production. Forces acting on the plunging flat plate are also estimated using DPIV data. The added-mass force acting on the plunging flat plate is analytically calculated and considered for the efficiency of the flapping.

In summary, the plunge cases exhibiting large thrust production, determined both qualitatively and quantitatively, also experience the largest added-mass forces. Eventually, the efficiency will be considerably degraded for those cases. However, the cases experiencing low added-mass forces are either on the drag occurrence side of the h-k plot or very close to the crossover from thrust to drag. On the other hand, it is difficult to determine experimentally the efficiency where it is expected to be high since drag measurement using load cells or drag estimation using non-intrusive flow diagnostics still suffer from unresolved issues.

Acknowledgements

This study is supported by EU under grant FP7- AAT- 2013- RTD-1, 605151 NIOPLEX (Non-intrusive Optical Pressure and Loads Extraction for Aerodynamic Analysis) and TUBITAK Grant 112M682 (Investigation of Flow Structures and Unsteady Loading for a Wing in Periodic or Transient Flapping Motion).

References

Anderson, J.M., Streitlien, K., Barrett, D.S., Triantafyllou, M.S., (1998). *Oscillating foils of high propulsive efficiency.* Journal of Fluid Mechanics Vol.360, pp.41-72

Betz, A., (1912). *Ein Beitrag zur Erklarung des Segelfluges*, Zeitschrift fur Flugtechnik und Motorluftschiffahrt, Vol. 3, pp. 269-272.

Bohl D.G.and Koocheshahani M.M. (2009). *MTV measurements of the vertical field in the wake of an airfoil oscillating at high reduced frequency*, J.Fluid Mech., Vol. 620, p:63-88.

Çaylan, U., Seçkin, S., Köse, C., Son, O., Zaloğlu, B., Fenercioğlu, İ., and Çetiner, O. (2014*). Çırpan kanatta üç boyutluluk etkisi.* Ulusal Havacılıkta İleri Teknolojiler Konferansı, HİTEK-2014-094.

Fenercioglu I, (2010). *Experimental Investigaton of Flow Structures around an Oscillating Airfoil in steady Current,* PhD Thesis, Istanbul Technical University

Fenercioglu, I., and Cetiner, O. (2012). *Categorization of flow structures around a pitching and plunging airfoil.* Journal of Fluids and Structures, Vol. 31, pp. 92-102.

Fenercioglu, I., and Cetiner, O. (2014). *Effect of unequal flapping frequencies on flow structures.* Aerospace Science and Technology, Vol. 35, pp. 39-53.

Jardin, T., Chatellier, L., Farcy, A. and David, L., (2009). *Correlation between vortex structures and unsteady loads for flapping motion in hover,* Experiments in Fluids Vol. 47, pp. 655-664.

Jones, K. D., Dohring, C. M., and Platzer, M.F., (1996). *Wake Structures Behind Plunging Airfoils: A comparison of Numerical and Experimental Results*, AIAA 96-007 (Reno, USA).

Jones, K.D., Dohring, C.M., Platzer, M.F., (1998). *Experimental and computational investigation of the Knoller-Betz effect*. AIAA Journal 36(7), 1240-1246

Karakaş, F., Paça , O., Köse, C., Son, O., Zaloğlu, B., Fenercioğlu, İ., and Çetiner, O. (2014). *Çırpan kanatta kanat profilinin etkisi* . Havacılık ve Uzay Teknolojileri Dergisi, Vol. 7(2), pp. 55-70.

Katzmayr, R., (1922). *Effect of Periodic Changes of Angle of Attack on Behavior of Airfoils*, NACA TM 147.

Knoller, R., (1909). *Die Gesetze des Luftwiderstandes*, Flug- und Motortechnik (Wien), Vol. 3, No. 21, pp. 1-7.

Kurtulus, F., Scarano, F. and David, L., (2007). Unsteady aerodynamic forces estimation on a square cylinder by TR-PIV, Experiments in Fluids Vol. 42, pp. 185-196.

Naudascher, E. and Rockwell, D., (2005). *Flow-Induced Vibrations: An Engineering Guide,* ISBN-13: 978-0486442822, Dover Publications.

Turam, E., Son, O. ve Çetiner, O., (2014). *DPIV verilerinden kuvvet elde edilmesinde deney parametreleri için hassasiyet analizi*, V. Ulusal Havacılık ve Uzay Konferansı (UHUK), UHUK-2014-112, 8-10 Eylül 2014, Erciyes Üniversitesi, Kayseri.

Tronchin, T., David, L. and Farcy, A., (2015). *Loads and pressure evaluation of the flow around a flapping wing from instantaneous 3D velocity measurements*, Experiments in Fluids 56:7, DOI 10.1007/s00348-014-1870-x.

URL: http://nioplex.eu/

van Oudheusden, BW, (2013). *PIV-based pressure measurement,* Measurement Science and Technology, Vol. 24, No.3, pp. 1-32.

Violato, D., Moore, P. and Scarano, F., (2011). *Lagrangian and Eulerian pressure field evaluation of rod-airfoil flow from time-resolved tomographic PIV*, Experiments in Fluids Vol. 50, pp. 1057-1070.